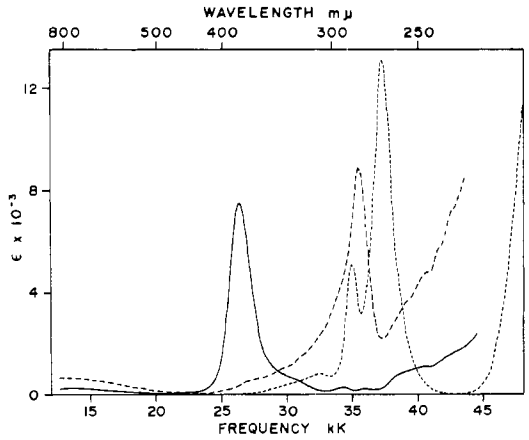

Figure 3. Polarized absorption spectra of $BaNi(CN)_4 \cdot 4H_2O$: —, out-of-plane: ––, in-plane on the (110) face; ---, solution spectrum of $Ni(CN)_4^{2-}$.

close correspondence of the ∥ and ⊥ directions with the out-of-plane and in-plane molecular directions, respectively (see Figure 1), allowed the transformed crystal ⊥ and ∥ spectra to be identified as in-plane and out-of-plane spectra, respectively. These spectra were adjusted for solution equivalency by multiplying the ∥ spectrum by $^1/_3$ and the ⊥ spectrum by $^2/_3$ to account for the fixed nature of the crystalline vs. the random orientation of the solvated species.

Results and Discussion

$BaNi(CN)_4 \cdot 4H_2O$ is known to be monoclinic with 45° staggered, stacked planes having normals 4° 46′ from the *c* axis.[15] We have determined, through correlating an *h*,*k*,0 Weissenberg photo with the crystal face orientations, that the elongated faces are (120) and (110). Figure 1 presents a stereoview of the crystal morphology with a single column of stacked $Ni(CN)_4^{2-}$ planes, viewed normal to the (110) plane. It is evident, from Figure 1, that the two faces present similar orientations of molecular planes and that one should expect similar spectra, as opposed to $CsKNi(CN)_4$ where planar orientations and thus spectra observed from adjacent faces are distinctly different.[11,16] The polarized specular reflectance from the (110) and (120) faces are shown in Figure 2, and, as expected, the corresponding spectra on each face are nearly identical. The greater reflectivity from the (110) face appears to be primarily due to the better surface quality of the crystals used for those spectra. The slight tilt of the normals from the *c* axis does not affect the apparent dichroism of the crystal, as is evident from the reflection spectra, where the large ∥ reflection at 26.0×10^3 cm^{-1} shows no component in the ⊥ direction.

The absorption-equivalent spectra, transformed from the reflection data on the (110) face, are shown in Figure 3 with the solution absorption spectrum of $Ni(CN)_4^{2-}$. The band at 26.1×10^3 cm^{-1} with an ϵ_{max} of 7130 in a region of no allowed solution transitions is evidence of a significant solid-state effect. This band, incidentally, seems to have been the cause of the high-energy opacity of the $BaNi(CN)_4 \cdot 4H_2O$ crystals in absorption studies.[8]

Since $BaNi(CN)_4 \cdot 4H_2O$ with a nickel–nickel distance of 3.36 Å is isomorphous with $BaPd(CN)_4 \cdot 4H_2O$ (Pd–Pd = 3.37 Å)[17] and $BaPt(CN)_4 \cdot 4H_2O$ (Pt–Pt = 3.32 Å),[18] it would be interesting to compare the solid-state bands in the three compounds. Since the degree of spectral shift has been recognized

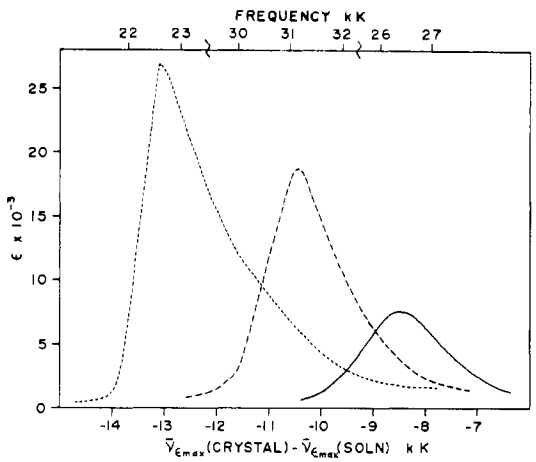

Figure 4. Out-of-plane polarized absorption spectra of solid-state band regions: $BaNi(CN)_4 \cdot 4H_2O$, —; $BaPd(CN)_4 \cdot 4H_2O$, ––; $BaPt(CN)_4 \cdot 4H_2O$, ---. The peak maxima are located according to the spectral shift upon crystallization. Pd and Pt data are from ref 7 and 9.

as an indication of the extent of solid-state perturbation, the bands will be positioned according to spectral shift upon crystallization. The solution origin of the solid-state band in $BaPd(CN)_4 \cdot 4H_2O$ has been found to be $\sim 41.6 \times 10^3$ cm^{-1},[7] for a spectral shift upon crystallization of $\sim -10.4 \times 10^3$ cm^{-1}. From polarization evidence on the unstacked (and unperturbed) tetracyanonickelate salt $CsKNi(CN)_4$[11] and following the results of a series of nickel glyoximes[19] and a series of $Pd(CN)_4 \cdot 4H_2O$ salts,[7] the out-of-plane polarized solution band at 34.9×10^3 cm^{-1}, which disappears upon crystallization, may be tentatively identified as the origin of the solid-state band in $BaNi(CN)_4 \cdot 4H_2O$, which would give a spectral shift of -8.1×10^3 cm^{-1}. The solution origin of the solid-state band in $BaPt(CN)_4 \cdot 4H_2O$ has been identified as being the peak at 35.7×10^3 cm^{-1},[7] for a spectral shift of -13.1×10^3 cm^{-1} upon crystallization. These three solid-state bands are plotted in Figure 4 with their maxima positioned according to these spectral shifts (lower abscissa). The individual bands are plotted as absorption coefficient vs. wavenumber (upper abscissa). The spectral shape and degree of shift in the nickel complex is consistent with the trend which appears to have been established in the platinum and palladium complexes, indicating that the solid-state effect in the three complexes is of a similar nature.

Acknowledgment. This work was partially supported by Research Corp. through a Cottrell College Science Grant, which is gratefully acknowledged.

Registry No. $BaNi(CN)_4 \cdot 4H_2O$, 17836-80-5.

(14) Anex, B. G. *Mol. Cryst.* **1966**, *1*, 1.
(15) Larsen, F. K.; Hazell, R. G.; Rasmussen, S. E. *Acta Chem. Scand.* **1969**, *23*, 61.
(16) Musselman, R. L.; Sanger, T. J., manuscript in preparation.
(17) Brasseur, H.; De Rassenfosse, A. *Bull. Soc. Fr. Mineral.* **1938**, *61*, 129.
(18) Maffly, R. L.; Johnson, P. L.; Williams, J. M. *Acta Crystallogr.* **1977**, *33*, 884.
(19) Anex, B. G.; Krist, F. K. *J. Am. Chem. Soc.*, **1967**, *89*, 6114.

Contribution from the Department of Chemistry, Seoul National University, Seoul, Korea

Kinetic Study of the Zinc Ion Catalyzed Hydrolysis of *O*-Acetyl-2-pyridinecarboxaldoxime

Junghun Suh,* Eun Lee, and Eun Sook Jang

Received September 18, 1980

A number of studies on metal ion catalyzed hydrolysis of esters have been reported and have provided valuable information on the roles of metal ions in hydrolytic metalloenzymes.[1,2] Metal ions are proposed to serve as superacids

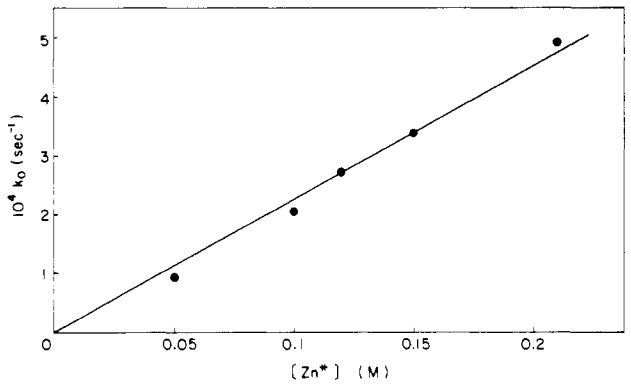

Figure 1. Plot of the pseudo-first-order rate constant (k_0) for the hydrolysis of **1** against [Zn^{2+}] measured at pH 5.09.

to polarize the scissile carbonyl group or to enhance the ionization and, consequently, the nucleophilicity of the metal-bound water. In addition, suitably coordinated metal ions can increase the leaving ability of the alcohol portion of the ester substrate. In an attempt to devise catalytic systems where these factors operate cooperatively, the zinc ion catalyzed hydrolysis of *O*-acetyl-2-pyridinecarboxaldoxime (**1**) has been

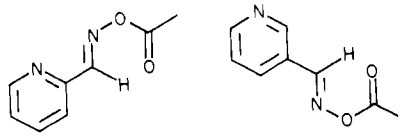

1 **2**

investigated. In this note, the catalytic ability and roles of the zinc ion in the reaction are described.

Experimental Section

Materials. *O*-Acetyl-2-pyridinecarboxaldoxime (**1**) and *O*-acetyl-3-pyridinecarboxaldoxime (**2**) were prepared as reported.[3] Zinc chloride ("ultrapure") was purchased from Alfa. Water was redistilled and deionized prior to use in the kinetic studies.

Kinetics. Reaction rates were measured with a thermojacketed Beckman Model 25 spectrophotometer. The temperature was controlled to within ±0.1 °C with a Haake E 52 circulator. pH measurements were performed with a Chemtrix Type 60 A pH meter.

Reactions were followed at 310 nm for **1** and 300 nm for **2**, for the conversion of the oxime esters to the oximes. Product spectra indicated that the reactions of **1** and **2** produced the corresponding oximes in equimolar amounts. Initial concentrations of **1** and **2** were 1.1×10^{-4} and 4.0×10^{-4} M, respectively. Ionic strength was adjusted with sodium chloride, and the buffer solutions contained 4-morpholineethanesulfonic acid. Reaction rates were not affected appreciably by the variation in the buffer concentration over 0.01–0.03 M. All of the reactions were carried out in the presence of 0.8 % (v/v) acetonitrile.

Results and Discussion

Rate Data. The pseudo-first-order rate constants (k_0) for the hydrolysis of **1** in the presence of various amounts of the zinc ion were measured at pH 5–7 and 25 °C. The concentration of the zinc ion was limited by its solubility. Within this range of [Zn^{2+}], k_0 was proportional to [Zn^{2+}] at a given pH. Sample rate data obtained at pH 5.09 are illustrated in Figure 1. The slopes of the plot of k_0 against [Zn^{2+}] was in turn proportional to [OH^-], indicating that the reaction is first order with respect to both [Zn^{2+}] and [OH^-]. The rate data obtained are summarized in Table I. The overall rate equation thus obtained was

$$k_0 = (1.7 \pm 0.1) \times 10^6[Zn^{2+}][OH^-]\ s^{-1} \quad (1)$$

Table I. Rate Data Obtained for the Zinc Ion Catalyzed Hydrolysis of **1**[a]

pH	[Zn^{2+}], M	$k_0/[Zn^{2+}][OH^-]$,[b] $10^6\ M^{-2}\ s^{-1}$	k_{cat}/k_{sp}[c]
7.00	0–0.01	1.71 ± 0.04	570
5.93	0–0.1	1.64 ± 0.05	1000
5.09	0–0.21	1.81 ± 0.04	220

[a] Measured at 25 °C and ionic strength 1.0. [b] The slope of the plot of k_0 against [Zn^{2+}] at a given pH was divided by [OH^-]. [c] The pseudo-first-order rate constant measured in the presence of zinc ion at the highest concentration indicated in the second column is denoted as k_{cat} and that for the corresponding spontaneous reaction as k_{sp}.

Table II. Effect of the Zinc Ion on the Hydrolysis of **1** and **2** at pH 7.0, 25 °C, and Ionic Strength 1.0

	k_0, s^{-1}		
	spontaneous[a] (k_{sp})	0.01 M Zn^{2+} added (k_{cat})	k_{cat}/k_{sp}
1	3.0×10^{-6}	1.7×10^{-3}	570
2	2.0×10^{-6}	2.6×10^{-5}	13

[a] Taken from the literature.[3]

Catalytic Efficiency. The pseudo-first-order rate constants obtained in the presence of zinc ion are compared with those (k_{sp}) of the corresponding spontaneous reactions in Table I. The values of k_{sp} were taken from the literature.[3] The rate enhancement caused by the addition of zinc ion is up to 1000-fold as indicated in the table.

Mechanism of Catalysis. The rate expression of eq 1 is compatible with both the direct attack (**3**) of the zinc-bound

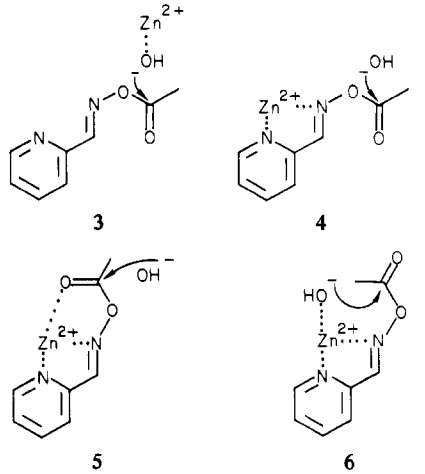

3 **4**

5 **6**

hydroxide ion to **1** and the mechanisms (**4**–**6**) involving the Zn^{2+}·**1** complex. The mechanism of **3** can be eliminated on the basis of the much smaller rate increase (Table II) caused by the zinc ion in the hydrolysis of **2** in which chelate formation with the zinc ion is not possible.

When the reaction proceeds through complex formation (eq 2), a saturation curve is expected for the plot of k_0 against

$$Zn^{2+} + \mathbf{1} \rightleftharpoons Zn^{2+}\cdot\mathbf{1} \xrightarrow{k'} \text{products} \quad (2)$$

[Zn^{2+}] (eq 3). However, k_0 is proportional to [Zn^{2+}] when

$$k_0 = k'K[Zn^{2+}]/(1 + K[Zn^{2+}]) \quad (3)$$

(1) Satchell, D. P. N.; Satchell, R. S. "Annual Reports on the Progress of Chemistry"; The Chemical Society: London, England, 1979; Vol. 75, Sect. A, pp 25–48 and references therein.
(2) Bender, M. L. "Mechanisms of Homogeneous Catalysis from Protons to Proteins"; Wiley-Interscience: New York, 1971; Chapter 8.
(3) Blanch, J. H. *J. Chem. Soc. B* **1968**, 167.

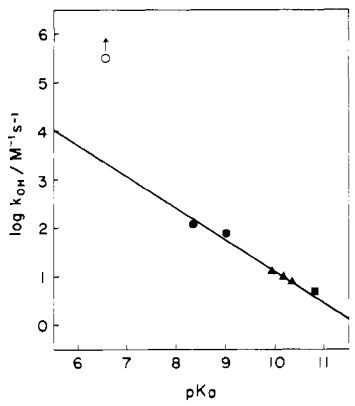

Figure 2. Plot of log k_{OH} against the pK_a of the leaving oxime for the alkaline hydrolysis of acetyl esters of various oximes measured at 25 °C. The pK_a values are taken from the literature.[5] The data presented are the rates for Zn^{2+}·**1**(O) and the acetyl esters of benzaldoxime[3] (■), 2-, 3-, or 4-pyridinecarboxaldoxime[3] (▲), and 3- or 4-(hydroxyimino)methyl-*N*-methylpyridinium internal salt[6] (●). The linear line has a slope (β_{LG}) of −0.65.

$K \ll 1/[Zn^{2+}]$, and the linearity seen in Figure 1 indicates $K \ll 5\ M^{-1}$. The small formation constant for Zn^{2+}·**1** can be ascribed to the low electron density on the nitrogens of **1**. The pK_a value for the pyridyl nitrogen of **1** was 2.29 ± 0.04 as measured by spectral titration (not shown).

Mechanisms compatible with the observed rate data and the complex formation are indicated in **4**–**6**. The only catalytic role of zinc ion proposed in **4** is to increase the leaving ability of the oxime ion (pK_a of the oxime is lowered from 10.04 to 6.52 upon complexation with zinc ion[4]). For the mechanism of **4**, k' of eq 2 represents the attack of the hydroxide ion on the complex ($k_{OH}[OH^-]$), and the corresponding pseudo-first-order rate constant under the condition of $K \ll 1/[Zn^{2+}]$ is

$$k_0 = k_{OH}K[Zn^{2+}][OH^-] \quad (4)$$

Comparison of eq 4 with eq 1 discloses $k_{OH} \gg 3 \times 10^5\ M^{-1}\ s^{-1}$ as $K \ll 5\ M^{-1}$. The plot of log k_{OH} against pK_a of the leaving oxime for the alkaline hydrolysis of various oxime esters is illustrated in Figure 2. The data point for Zn^{2+}·**1** represents the lowest limit estimated above. The large deviation seen with the data point for Zn^{2+}·**1** indicates that other catalytic factors in addition to simple decrease in the basicity of the leaving group is needed to explain the high reactivity of Zn^{2+}·**1**.

The most probable mechanism is, therefore, that of **5** or **6**. In these mechanisms, polarization of the carbonyl group by the zinc ion and the nucleophilic attack by the neighboring zinc-bound hydroxide ion are also proposed. These two factors have been proposed in several other instances,[7] although differentiation between them has not been successful.

In summary, the zinc ion catalyzed hydrolysis of **1** involves two cooperative catalytic factors: increased leaving ability of the oxime and enhanced nucleophilic attack of the hydroxide ion at the carbonyl carbon.

Acknowledgment. This investigation was supported by a grant from the Korean Science and Engineering Foundation.

Registry No. **1**, 19433-10-4; **2**, 19433-11-5; Zn^{2+}, 23713-49-7.

(4) Breslow, R.; Chapman, D. *J. Am. Chem. Soc.* **1965**, *87*, 4195.
(5) Blanch, J. H. *J. Chem. Soc. B* **1966**, 937.
(6) Blanch, J. H.; Onsager, O. T. *J. Chem. Soc.* **1965**, 3729.
(7) Fife, T. H.; Przystas, T. J.; Squillacote, V. L. *J. Am. Chem. Soc.* **1979**, *101*, 3017.

Contribution from the Department of Macromolecular Science, Faculty of Science, Osaka University, Toyonaka, Osaka 560, Japan, and Faculty of Pharmaceutical Science, Tokushima University, Tokushima 770, Japan

Raman and Resonance Raman Spectra of Oxomolybdenum(VI) and -(V) Complexes of Cysteine and Related Thiolate Ligands[1]

Norikazu Ueyama,[2] Michio Nakata,[2a] Takeo Araki,[2a] Akira Nakamura,*[2a] Shinsuke Yamashita,[2b] and Takuya Yamashita[2b]

Received June 20, 1980

Active sites of molybdoenzymes were recently investigated by X-ray absorption edges and EXAFS to reveal the nature of coordinating atoms around the molybdenum.[3] The oxidases, e.g., xanthine oxidase, were found to involve Mo=O and Mo—thiolate bonds. The coexistence of the hard (oxo) and soft (thiolate) ligands on the same molybdenum(VI) ion has been considered responsible for their high catalytic activity in O atom transfer oxidations and dehydrogenations. Stiefel et al. actively synthesized structural models of such enzymes.[4] By contrast, the active site of nitrogenase has no Mo=O moiety and consists of MoFe-mixed sulfur cluster where bridging inorganic sulfides (sulfido ligand) play an important role.[5]

We have prepared a series of oxomolybdenum complexes of cysteine-containing oligopeptides and here the Mo=O, Mo—S—Mo, and Mo—S—CH_2 bondings were investigated by Raman and resonance Raman spectra. These techniques have a distinct advantage over the infrared spectra in that information about vicinity of heavy-metal and sulfur atoms can be obtained. The resonance Raman spectra can detect presence of metal–metal or metal–sulfur bonds even in dilute aqueous solutions.

When one considers importance of the sulfur coordination at the molybdenum enzyme active sites, a correct assignment of Mo=O, Mo—S—Mo, or Mo—S—CH_2 vibrations in some relevant model complexes will contribute to further investigation and understanding of the enzymes.

Experimental Section

The dioxobis(acetylacetonato)molybdenum(VI) was purchased from Nakarai Chemical Co. The dioxomolybdenum(VI) complexes of cysteine methyl ester and cysteine ethyl ester were prepared by the method reported by Kay and Mitchell.[6] Dioxobis(benzyl cysteinato-*S*)molybdenum(VI), MoO_2(cysOBzl)$_2$, was synthesized by the following method. L-Cysteine benzyl ester hydrochloride (0.36 g) which was prepared by the procedure of Erlanger et al.[7] was dissolved in 1 mL of water. The solution was added to 1-mL aqueous solution of Na_2MoO_4 (0.21 g). A yellow precipitate was collected, washed with water, and dried over P_2O_5 under reduced pressure. Anal. Cald for $C_{20}H_{24}N_2O_6S_2Mo$: C, 43.80; H, 4.41; N, 5.11. Found: C, 43.2; H, 4.39; N, 5.01. Dioxobis(isopropyl cysteinato-*S*)molybdenum(VI), MoO_2(cysO-*i*-Pr)$_2$, was synthesized by the same method mentioned above for the MoO_2(cysOBzl)$_2$. Anal. Calcd for $C_{12}H_{24}N_2O_6S_2Mo$: C, 31.86; H, 5.35; N, 6.19. Found: C, 31.56; H, 5.35; N, 6.40. The dioxomolybdenum(VI) complexes of dimethyldithiocarbamato ($S_2CNMe_2^-$) and diethyldithiocarbamato ($S_2CNEt_2^-$) ligands were

(1) A part of the present paper has been communicated before: Ueyama, N.; Nakata, M.; Araki, T.; Nakamura, A.; Yamashita, S.; Yamashita, T. *Chem. Lett.* **1979**, 421.
(2) (a) Osaka University. (b) Tokushima University.
(3) Cramer, S. P.; Gillum, W. O.; Hodgson, K. O.; Mortenson, L. E.; Stiefel, E. I.; Chisnell, J. R.; Brill, W. J.; Shah, V. K. *J. Am. Chem. Soc.* **1978**, *100*, 3814.
(4) Stiefel, E. I. "Molybdenum and Molybdenum-Containing Enzymes"; Coughlan, M., Ed.; Pergamon Press: London, 1980.
(5) Cramer, S. P.; Hodgson, K. O.; Gillum, W. O.; Mortenson, L. E. *J. Am. Chem. Soc.* **1978**, *100*, 3398.
(6) Kay, A.; Mitchell, P. C. H. *J. Chem. Soc. A* **1970**, 2421.
(7) Erlanger, B. F.; Hall, R. H. *J. Am. Chem. Soc.* **1954**, *76*, 5781.

0020-1669/81/1320-1934$01.25/0